Differential constitutive equations for polymer melts : the extended Pom-Pom model

Differential constitutive equations for polymer melts: The extended Pom–Pom model

Wilco M. H. Verbeeten, Gerrit W. M. Peters,[a] and Frank P. T. Baaijens

Materials Technology, Faculty of Mechanical Engineering, Eindhoven University of Technology, P.O. Box 513, 5600 MB Eindhoven, The Netherlands

(Received 22 March 2000; final revision received 1 May 2001)

Synopsis

The *Pom–Pom* model, recently introduced by McLeish and Larson [J. Rheol. **42**, 81–110 (1998)], is a breakthrough in the field of viscoelastic constitutive equations. With this model, a correct nonlinear behavior in both elongation and shear is accomplished. The original differential equations, improved with local branch-point displacement, are modified to overcome three drawbacks: solutions in steady state elongation show discontinuities, the equation for orientation is unbounded for high strain rates, the model does not have a second normal stress difference in shear. The modified *extended Pom–Pom* model does not show the three problems and is easy for implementation in finite element packages, because it is written as a single equation. Quantitative agreement is shown with experimental data in uniaxial, planar, equibiaxial elongation as well as shear, reversed flow and step-strain for two commercial low density polyethylene (LDPE) melts and one high density polyethylene (HDPE) melt. Such a good agreement over a full range of well defined rheometric experiments, i.e., shear, including reversed flow for one LDPE melt, and different elongational flows, is exceptional. © *2001 The Society of Rheology.*
[DOI: 10.1122/1.1380426]

I. INTRODUCTION

A main problem in constitutive modeling for the rheology of polymer melts is to get a correct nonlinear behavior in both elongation and shear. Most well-known constitutive models, such as the PTT, Giesekus, and K-BKZ models, are unable to overcome this difficulty. Recently, McLeish and Larson (1998) have introduced a new constitutive model, which is a major step forward in solving this problem: the *Pom–Pom* model.

The rheological properties of entangled polymer melts depend on the topological structure of the polymer molecules. Therefore, the *Pom–Pom* model is based on the tube theory and a simplified topology of branched molecules. The model consists of two decoupled equations: one for the orientation and one for the stretch. A key feature is the separation of relaxation times for this stretch and orientation. Both an integral and a differential form are available.

After its introduction, the model has been intensively investigated. Bishko *et al.* (1999) presented calculations of the transient flow of branched polymer melts through a planar 4:1 contraction. For various LDPE samples, Inkson *et al.* (1999) showed predictions for a multimode version of the *Pom–Pom* model. Blackwell *et al.* (2000) suggested a modification of the model and introduced local branch-point withdrawal before the

[a]Author to whom correspondence should be addressed. Electronic mail: gerrit@wfw.wtb.tue.nl

molecules are fully stretched. Investigation of the thermodynamic admissibility of the differential *Pom–Pom* model was presented by Öttinger (2000). Although the model is found to be thermodynamically admissible, he showed that nonequilibrium thermodynamics strongly suggests several model modifications.

This paper investigates the differential form of the *Pom–Pom* model. Following the ideas of Blackwell *et al.* (2000), local branch-point displacement before maximum stretching is introduced by an exponential drop of the stretch relaxation times. Moreover, as adopted from Inkson *et al.* (1999), the structure is decoupled into an equivalent set of *Pom–Pom* molecules with a range of relaxation times and arm numbers: a multimode approach. However, three problems can still be detected. First, as the orientation equation is UCM-like, it is unbounded for high strain rates. Second, although local branch-point displacement is introduced, solutions in steady state elongation still show discontinuities due to the finite extensibility condition. And finally, this differential version does not have a second normal stress difference in shear. In Sec. II, we will introduce the *extended Pom–Pom* model that overcomes these problems.

Section III shows the results in a single-mode dimensionless form for both transient and steady state shear as well as elongational deformations. In Sec. IV, the multimode version is tested for two commercial LDPE melts. Both LDPE melts have been characterized thoroughly [Hachmann (1996); Kraft (1996); Meissner (1972, 1975); Münstedt and Laun (1979)], providing a large set of experimental data. To investigate the ability of the model to predict the rheological behavior of a melt with a different sort of topology (nonbranched), the experimental data of a HDPE melt is compared with the results of the multimode *Pom–Pom* model.

In short, the key objective of this work is to investigate the capabilities of an extended version of the *Pom–Pom* model to describe a wide range of available rheometric data for three different polyethylene melts.

II. THE DIFFERENTIAL POM–POM MODEL

To describe stresses of polymer melts, the Cauchy stress tensor σ is defined as

$$\sigma = -pI + 2\eta_s D + \sum_{i=1}^{M} \tau_i . \tag{1}$$

Here, p is the pressure term, I is the unit tensor, η_s denotes the viscosity of the purely viscous (or solvent) mode, $D = 1/2(L + L^T)$ the rate of deformation tensor, in which $L = (\nabla \mathbf{u})^T$ is the velocity gradient tensor and $(\cdot)^T$ denotes the transpose of a tensor. The viscoelastic contribution of the ith relaxation mode is denoted by τ_i and M is the total number of different modes. A multimode approximation of the relaxation spectrum is often necessary for a realistic description of the viscoelastic contributions.

Here, the constitutive behavior for a single mode of the viscoelastic contribution is described with the differential *Pom–Pom* model. A schematic structure of the molecule for this model is given in Fig. 1. The model is developed, mainly, for long-chain branched polymers. The multiple branched molecule can be broken down into several individual modes [Inkson *et al.* (1999)]. Each mode is represented by a backbone between two branch points, with a number of dangling arms on every end. The backbone is confined by a tube formed by other backbones. For details refer to McLeish and Larson (1998). The original differential form by McLeish and Larson (1998), improved with local branch-point displacement [Blackwell *et al.* (2000)], is written in two decoupled equations and reads as follows:

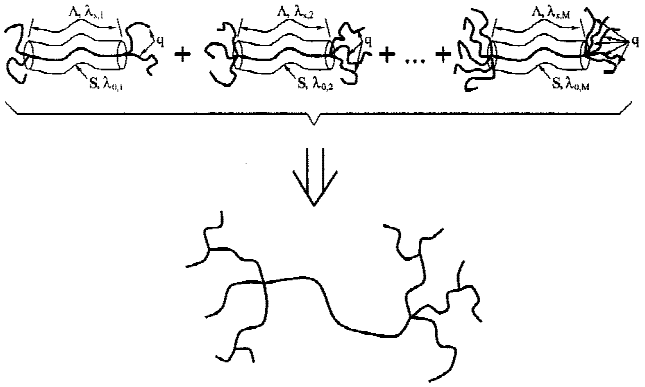

FIG. 1. Schematic structure of the *Pom–Pom* "molecule."

$$\overset{\nabla}{A}+\frac{1}{\lambda_{0b}}\left(A-\frac{1}{3}I\right)=0,\quad S=\frac{A}{I_A}, \tag{2}$$

$$\Lambda=\Lambda(D{:}S)-\frac{1}{\lambda_s}(\Lambda-1),\quad \lambda_s=\lambda_{0s}e^{-\nu(\Lambda-1)}\quad \forall\Lambda\leqslant q, \tag{3}$$

$$\tau=\sigma-G_0I=G_0(3\Lambda^2S-I). \tag{4}$$

Expression (4) for the extra stress, differs (by a constant) from that proposed by McLeish and Larson (1998), but Rubio and Wagner (1999) have shown that for the differential model (4) is the correct form. Equations (2) and (3) are the evolution of orientation tensor S and backbone tube stretch Λ, respectively. A is an auxiliary tensor to get the backbone tube orientation tensor S. λ_{0b} is the relaxation time of the backbone tube orientation. It is obtained from the linear relaxation spectrum determined by dynamic measurements. I_A is the first invariant of tensor A, defined as the trace of the tensor: $I_A=\mathrm{tr}(A)$. The backbone tube stretch Λ is defined as the length of the backbone tube divided by the length at equilibrium. λ_0 is the relaxation time for the stretch, and ν a parameter which, based on the ideas of Blackwell *et al.* (2000), is taken to be $2/q$, where q is the amount of arms at the end of a backbone. Alternatively, ν can also be seen as a measure of the influence of the surrounding polymer chains on the backbone tube stretch. Finally, G_0 is the plateau modulus, also obtained from the linear relaxation spectrum. The upper convected time derivative of the auxiliary tensor $A\nabla$ is defined as

$$\overset{\nabla}{A}=\dot{A}-L\cdot A-A\cdot L^T=\frac{\partial A}{\partial t}+\mathbf{u}\cdot\nabla A-LA-AL^T. \tag{5}$$

The reason for introducing an auxiliary tensor A in Eq. (2) is to obtain an orientation tensor S that mimics the behavior of the true tube orientation, given by the integral expression [see McLeish and Larson (1998)]. For clarification (and also to compare more easily with our model modifications later on), the equation is rewritten in terms of S (see also Appendix A)

$$\overset{\nabla}{S}+2(D{:}S)S+\frac{1}{\lambda_{0b}I_A}\left(S-\frac{1}{3}I\right)=0. \tag{6}$$

Notice that this equation is almost identical to Eq. (30) in McLeish and Larson (1998), i.e., the simplest candidate for the backbone evolution that they ruled out

$$\overset{\nabla}{S}+2(D:S)S+\frac{1}{\lambda_{0b}}\left(S-\frac{1}{3}I\right)=0. \tag{7}$$

In fact, introducing the auxiliary tensor **A** is equivalent to multiplying the backbone relaxation time with I_A in this simplest candidate. Although the shear-response S_{12} of Eq. (7) does have a maximum as a function of shear rate, it decreases as $\gamma^{-2/3}$ rather than as γ^{-1} which is found for the integral form and Eqs. (2) and (6). The latter is the shear thinning behavior in standard Doi–Edwards theory for linear polymers. If local branch-point displacement is not accounted for, the less steep shear-rate dependence does not give the right shear-thinning response. In Sec. IV, the positive influence of local branch-point displacement on the shear-thinning behavior will be shown. In short, Eqs. (2) and (6) are equivalent and have similar asymptotic forms in extension and shear as the integral version, contrary to Eq. (7). A disadvantage is that Eq. (2) is UCM-like: it runs into numerical problems when trying to solve it for high elongation rates ($\dot{\varepsilon}\lambda_{0b} > 1$). The UCM-type models are unbounded in extension.

Notice, that Eq. (3) holds only if the stretch Λ is smaller or equal to the number of dangling arms q. In this way, finite extensibility of the backbone tube is introduced. However, this condition causes discontinuities in steady state elongational viscosity curves. Although local branch-point displacement diminishes this discontinuity, it is still present.

Unfortunately, the set of Eqs. (2)–(4) predicts a zero second normal stress coefficient in shear ($\Psi_2 = 0$). There are several reasons to include a second normal stress difference. First of all, experimental data [Kalogrianitis and van Egmond (1997)] indicates a nonzero Ψ_2. Larson (1992) showed that a nonzero Ψ_2 positively influences the stability of viscoelastic flows. Debbaut and Dooley (1999) observed and analyzed the secondary motions due to the nonzero second normal stress difference. Furthermore, during flow-induced crystallization, phenomena have been observed that are assumed to be related to the second normal stress difference [Jerschow and Janeschitz-Kriegl (1996)]. Doufas *et al.* (1999) introduced a model for flow-induced crystallization that incorporates $\Psi_2 \neq 0$.

A number of changes are made to the original differential equations to overcome these disadvantages. The extended model is based on the molecular background of the original *Pom–Pom* model. In particular the different relaxation processes for stretch and orientation are maintained. However, the requirement that the tube orientation for linear polymers follows the Doi–Edwards theory is relaxed. Moreover, the phenomenological approach of Inkson *et al.* (1999) is followed in the sense that the model parameters will not be determined from molecular data directly.

A different starting point is taken. The polymer melt molecules will be represented by connector vectors $\mathbf{R}_i$, similar to Peters and Baaijens (1997). Consider a single *Pom–Pom* molecule as given in Fig. 2. A part of the backbone tube of the molecule is defined as the dimensionless connector vector $\mathbf{R}_i$, with a dimensionless length or stretch Λ_i and direction $\mathbf{n}_i$:

$$\mathbf{R}_i = |\mathbf{R}_i|\mathbf{n}_i = \Lambda_i\mathbf{n}_i. \tag{8}$$

The subscript i is introduced to distinguish between different parts. For convenience, it will be omitted in the rest of the paper. The equation of motion for a vector **R** is postulated as

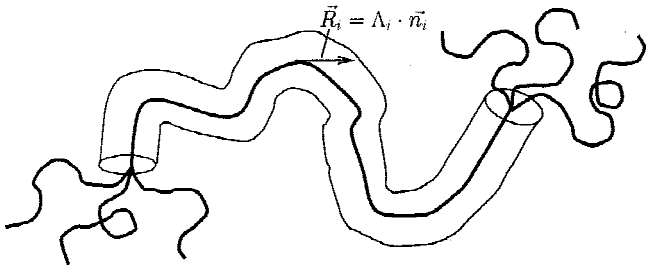

FIG. 2. Connector vector $\mathbf{R}_i$ for a backbone-tube part of an arbitrary molecule.

$$\mathbf{R} = (L-B)\mathbf{R} \Rightarrow \mathbf{n} = (L-B)\mathbf{n} - (D-B):(\mathbf{nn})\mathbf{n}, \tag{9}$$

where the second order tensor B is a yet to be specified function of averaged, thus macroscopic, variables, i.e., the stress, strain or strain rate. The level of description is taken in averaged sense. The term $-B\mathbf{R}$ represents the slippage of the element with respect to the continuum. Therefore, the tensor B is called the slip tensor.

Now, let us define the orientation tensor S as

$$S = \langle \mathbf{nn} \rangle, \tag{10}$$

where $\langle \cdot \rangle$ denotes an average over the distribution space. Then its time derivative is taken (which is not trivial as it is a time derivative of an integral over the distribution space)

$$\dot{S} = \langle \dot{\mathbf{n}}\mathbf{n} + \mathbf{n}\dot{\mathbf{n}} \rangle. \tag{11}$$

By using the closure approximation $\langle \mathbf{nnnn} \rangle = \langle \mathbf{nn} \rangle \langle \mathbf{nn} \rangle$, this gives

$$\overset{\nabla}{S} + B \cdot S + S \cdot B^T + 2[(D-B):S]S = 0. \tag{12}$$

In a similar way, take the evolution in time of the length of an arbitrary averaged connector vector $|\mathbf{R}|$:

$$|\dot{\mathbf{R}}| = \dot{\Lambda} = \Lambda(D-B):\langle \mathbf{nn} \rangle \Leftrightarrow \dot{\Lambda} = \Lambda(D-B):S, \tag{13}$$

stating that any local fluctuations in the stretch Λ very rapidly equilibrate over the backbone tube [McLeish and Larson (1998)], i.e., $\Lambda_i = \Lambda_j = \Lambda \forall i,j$.

What remains is a choice for the slip tensor B. We choose it to be only a function of the averaged macroscopic stress σ [as defined by Eq. (4)]:

$$B = c_1\sigma + c_2 I - c_3\sigma^{-1} = c_1 3G_0\Lambda^2 S + c_2 I - \frac{c_3}{3G_0\Lambda^2}S^{-1}, \tag{14}$$

with c_1, c_2, and c_3 still to be specified. If Eq. (14) is substituted into Eq. (12), the orientation equation is only a function of c_1 and c_3. To incorporate a non-zero second normal stress coefficient that is modeled by anisotropic relaxation, we choose c_1 and c_3 to be Giesekus-like [see, e.g., Eq. (A10) in Peters and Baaijens (1997)]:

$$c_1 = \frac{\alpha}{2G_0\lambda_{0b}}, \quad c_3 = \frac{G_0(1-\alpha)}{2\lambda_{0b}}. \tag{15}$$

Here, α is a material parameter ($\alpha \geqslant 0$), defining the amount of anisotropy. To obey exactly the stretch Eq. (3) of McLeish and Larson, c_2 can be determined by substituting Eq. (14) into Eq. (13):

$$c_2 = \frac{1-\alpha-3\alpha\Lambda^4 I_{s\cdot s}}{2\lambda_{0b}\Lambda^2} + \frac{1}{\lambda_s}\left(1-\frac{1}{\Lambda}\right). \tag{16}$$

The slip tensor **B** then reads

$$B = \frac{3\alpha\Lambda^2}{2\lambda_{0b}} S + \left[\frac{1-\alpha-3\alpha\Lambda^4 I_{s\cdot s}}{2\lambda_{0b}\Lambda^2} + \frac{1}{\lambda_s}\left(1-\frac{1}{\Lambda}\right)\right] I - \frac{(1-\alpha)}{6\lambda_{0b}\Lambda^2} S^{-1}, \tag{17}$$

giving the evolution equations for orientation and stretch

$$\overset{\nabla}{S} + 2(D:S)S + \frac{1}{\lambda_{0b}\Lambda^2}\left[3\alpha\Lambda^4 S\cdot S + (1-\alpha-3\alpha\Lambda^4 I_{s\cdot s})S - \frac{(1-\alpha)}{3} I\right] = 0, \tag{18}$$

and

$$\dot{\Lambda} = \Lambda(D:S) - \frac{1}{\lambda_s}(\Lambda-1), \quad \lambda_s = \lambda_{0s} e^{-\nu(\Lambda-1)}. \tag{19}$$

For nonzero α, also a nonzero second normal stress coefficient Ψ_2 is predicted. Moreover, Ψ_2 is proportional to α. If $\alpha = 0$, Eq. (18) simplifies to

$$\overset{\nabla}{S} + 2(D:S)S + \frac{1}{\lambda_{0b}\Lambda^2}\left(S - \frac{1}{3} I\right) = 0. \tag{20}$$

Notice, that this equation is equivalent to Eq. (6) of McLeish and Larson, with the only difference that I_A is replaced by Λ^2. Thus, to end up with the Eqs. (2) or (6) and (3), as was derived by McLeish and Larson (1998), the slip tensor B, to be filled in Eqs. (12) and (13), reads

$$B = \left[\frac{1}{2\lambda_{0b} I_A} + \frac{1}{\lambda_s}\left(1-\frac{1}{\Lambda}\right)\right] I - \frac{1}{6\lambda_{0b} I_A} S^{-1}. \tag{21}$$

In this way, we have shown that our approach is consistent with McLeish and Larson (1998), and the same equations can be found.

The earlier model may be reformulated into a single equation. For this purpose, the evolution equation for the extra stress tensor τ will be written in terms of the slip tensor **B**. To achieve that, we choose to work with tensor c, which is the average of all the connector vectors **R** over the distribution space, also known as the conformation tensor. Now it follows:

$$c = \langle \mathbf{RR} \rangle = \langle \Lambda\mathbf{n}\Lambda\mathbf{n} \rangle = \Lambda^2 \langle \mathbf{nn} \rangle = \Lambda^2 S = I_c S \Rightarrow I_c = \Lambda^2. \tag{22}$$

For the extra stress, it can now be written

$$\tau = 3G_0 c - G_0 I = 3G_0 \langle \mathbf{RR} \rangle - G_0 I = 3G_0 \Lambda^2 S - G_0 I, \tag{23}$$

which is similar to Eq. (4). By taking the time evolution of the previous equation, it follows:

$$\dot{\tau} = 3G_0 \langle \dot{\mathbf{R}}\mathbf{R} + \mathbf{R}\dot{\mathbf{R}} \rangle. \tag{24}$$

The stress evolution equation then reads

$$\overset{\nabla}{\tau}+B\cdot\tau+\tau\cdot B^T+G_0(B+B^T)=2G_0D. \tag{25}$$

Substituting Eq. (17) into Eq. (25) gives the single equation for τ:

$$\overset{\nabla}{\tau}+\lambda(\tau)^{-1}\tau=2G_0D, \tag{26}$$

with

$$\lambda(\tau)^{-1}=\frac{1}{\lambda_{0b}}\left\{\frac{\alpha}{G_0}\tau+f(\tau)^{-1}I+G_0\underbrace{[f(\tau)^{-1}-1]}_{(a)}\tau^{-1}\right\}, \tag{27}$$

$$\frac{1}{\lambda_{0b}}f(\tau)^{-1}=\underbrace{\frac{2}{\lambda_s}\left(1-\frac{1}{\Lambda}\right)}_{(b)}+\underbrace{\frac{1}{\lambda_{0b}\Lambda^2}\left(1-\frac{\alpha I_{\tau\cdot\tau}}{3G_0^2}\right)}_{(c)}, \tag{28}$$

and

$$\Lambda=\sqrt{1+\frac{I_\tau}{3G_0}},\quad \lambda_s=\lambda_{0s}e^{-\nu(\Lambda-1)},\quad \nu=\frac{2}{q}. \tag{29}$$

Notice, that we drop the finite extensibility condition of Eq. (3) ($\Lambda \leqslant q$). McLeish and Larson (1998) suggest, that the backbone tube stretch equation only holds if the stretch Λ is smaller than the amount of arms q. The backbone can only maintain a maximum stretch, which is equal to the number of arms ($\Lambda = q$). However, Eq. (3) is the evolution for the averaged backbone tube stretch. So, some molecules will have reached their maximum stretch before others, giving a maximum stretch distribution. As the finite extensibility condition does not yield a distribution but a discrete condition, it seems to be unphysical, especially if polydispersity is involved. Even in case of monodispersity, such a discrete behavior is not seen in data [Blackwell *et al.* (2000)]. Moreover, the condition produces an unrealistic discontinuity in the gradient of the extensional viscosity [McLeish and Larson (1998); Bishko *et al.* (1999); Inkson *et al.* (1999); Blackwell *et al.* (2000)]. Therefore, the sudden transition from stretch dynamics to a fixed maximum stretch has been taken out. It can also be justified by considering that local branch-point displacement contributes to a larger backbone tube, which again can be stretched further. Taking away the finite extensibility condition results in the removal of the peaks and discontinuities of steady state elongational curves, as will be shown in the next section, while the stretch is not unbounded. This because the exponential in the stretch relaxation time [$e^{-\nu(\Lambda-1)}$] ensures for high strains, that the stretch relaxes very fast and stays bounded. The parameter q still denotes a measure for the amount of arms in the molecule for a particular mode. However, q does not fix the finite extensibility, but only limits it indirectly by influencing the drop in the stretch relaxation time λ_s.

Although two effects, stretch and orientation, are combined in one equation, the different parts can still be recognized. Assume the easy case that $\alpha = 0$. For low strains, i.e., no stretch ($\Lambda = 1$), part (b) in Eq. (28) equals zero and the only relaxation time of significance is the one for the backbone tube orientation λ_{0b}. In that case, part (a) in Eq. (27) is also equal to zero and this equation reduces to the linear viscoelastic model. For high strains, i.e., significant stretch ($\Lambda \gg 1$), part (c) in Eq. (28) reduces to zero and the stretch relaxation time λ_s becomes the most important relaxing mechanism. Physically, it could be interpreted as if the orientation can not relax because it is trapped by the

TABLE I. Double-equation XPP equation set.

Double-equation XPP model
Viscoelastic stress
$$\tau = G_0(3\Lambda^2 S - I).$$
Evolution of orientation
$$\overset{\nabla}{S} + 2[D:S]S + \frac{1}{\lambda_{0b}\Lambda^2}\left[3\alpha\Lambda^4 S\cdot S + (1-\alpha-3\alpha\Lambda^4 I_{S\cdot S})S - \frac{(1-\alpha)}{3}I\right] = 0.$$
Evolution of the backbone stretch
$$\dot{\Lambda} = \Lambda[D:S] - \frac{1}{\lambda_s}(\Lambda - 1), \quad \lambda_s = \lambda_{0s}e^{-\nu(\Lambda-1)}, \quad \nu = \frac{2}{q}.$$

stretching effect, and the stretch has to relax before the orientation is able to relax. Parameter α only influences the orientation part (c) of the equation.

The set of Eq. (18), (19), and (4) or Eq. (26) is referred to as the *extended Pom–Pom* (XPP) model, as, by choosing $\alpha \neq 0$, the model is extended with a second normal stress coefficient Ψ_2. This model overcomes the three problems mentioned earlier. For convenience, an overview of the model is given in Tables I and II.

Recently, Öttinger (2000) investigated the thermodynamic admissibility of the *Pom–Pom* model. He focused on the differential version, as it fits more naturally into the modern framework of nonequilibrium thermodynamics. He proposed a modification for the orientation equation, which also has a quadratic term in the orientation tensor. Similar as before, the model proposed by Öttinger (2000) can be written in a double-equation or single-equation formulation. (See Appendix B for details.)

III. MODEL FEATURES

A one mode version of the XPP model derived in the previous section will now be investigated for different simple flows. All variables are made dimensionless with G_0 and λ_{0b}. The parameters are chosen $q = 5$ and $\lambda_{0a} = (150/912)\lambda_{0b}$, unless indicated otherwise, i.e., the same choice as McLeish and Larson (1998) and Blackwell *et al.* (2000). The parameter related to the anisotropy, α, is varied to investigate its influence.

A. Simple shear

The transient and steady state viscosity, transient second over first normal stress coefficient ratio $(-\Psi_2/\Psi_1)$, steady state shear orientation S_{12}, and transient backbone stretch Λ for simple shear are plotted in Fig. 3.

The influence of α on η is rather small. Only for $\alpha = 0.5$, a small difference can be noted. The parameter α mostly influences Ψ_2. For $\alpha = 0$, clearly $-\Psi_2/\Psi_1 = 0$ and no line is plotted in that case.

The shear orientation S_{12} decreases as $\gamma^{-1/2}$ for high shear rates, as can be seen in the bottom plot of Fig. 3. However, the backbone stretch Λ does not increase dramatically fast, which is due to the local branch-point displacement that decreases the stretch relaxation time λ_s. Therefore, shear-thinning behavior is still accounted for, as is apparent from the steady state shear viscosity plot. The transient backbone stretch in Fig. 3 shows the characteristic overshoot.

TABLE II. Single-equation XPP equation set.

Single-equation XPP model
Viscoelastic stress
$\overset{\nabla}{\tau}+\lambda(\tau)^{-1}\tau = 2G_0 D.$
Relaxation time tensor
$\lambda(\tau)^{-1} = \frac{1}{\lambda_{0b}}\left\{\frac{\alpha}{G_0}\tau+f(\tau)^{-1}I+G_0[f(\tau)^{-1}-1]\tau^{-1}\right\}.$
Extra function
$\frac{1}{\lambda_{0b}}f(\tau)^{-1} = \frac{2}{\lambda_s}\left(1-\frac{1}{\Lambda}\right)+\frac{1}{\lambda_{0b}\Lambda^2}\left(1-\frac{\alpha I_{\tau\tau}}{3G_0^2}\right).$
Backbone stretch and stretch relaxation time
$\Lambda = \sqrt{1+\frac{I_\tau}{3G_0}}, \quad \lambda_s = \lambda_{0s}e^{-\nu(\Lambda-1)}, \quad \nu = \frac{2}{q}.$

Figures for the transient and steady state first normal stress coefficient, steady state second over first normal stress coefficient ratio, steady state orientation components and steady state backbone stretch can be found in EPAPS Document No. E-JORHD2-45-013104.

B. Planar elongation

In Fig. 4 the transient and steady state first planar viscosity, transient second planar viscosity, and backbone stretch are shown for the model. The first planar viscosity is defined as

$$\eta_{p1} = \frac{\tau_{11}-\tau_{33}}{\varepsilon}, \tag{30}$$

while the second planar viscosity is given by

$$\eta_{p2} = \frac{\tau_{22}-\tau_{33}}{\varepsilon}. \tag{31}$$

The parameter α has almost no influence on the first planar viscosity, but a significant influence on the second planar viscosity.

Notice that the steady state planar viscosity is a smooth function with no peaks. This is due to the absence of a finite extensibility condition.

Different from simple shear, the transient backbone stretch shows no overshoot and reaches its steady state value right away. The steady state backbone stretch increases monotonically, but not drastically, due to local branch-point displacement.

Additional figures for the viscosity, orientation components and stretch can be found in EPAPS Document No. E-JORHD2-45-013104.

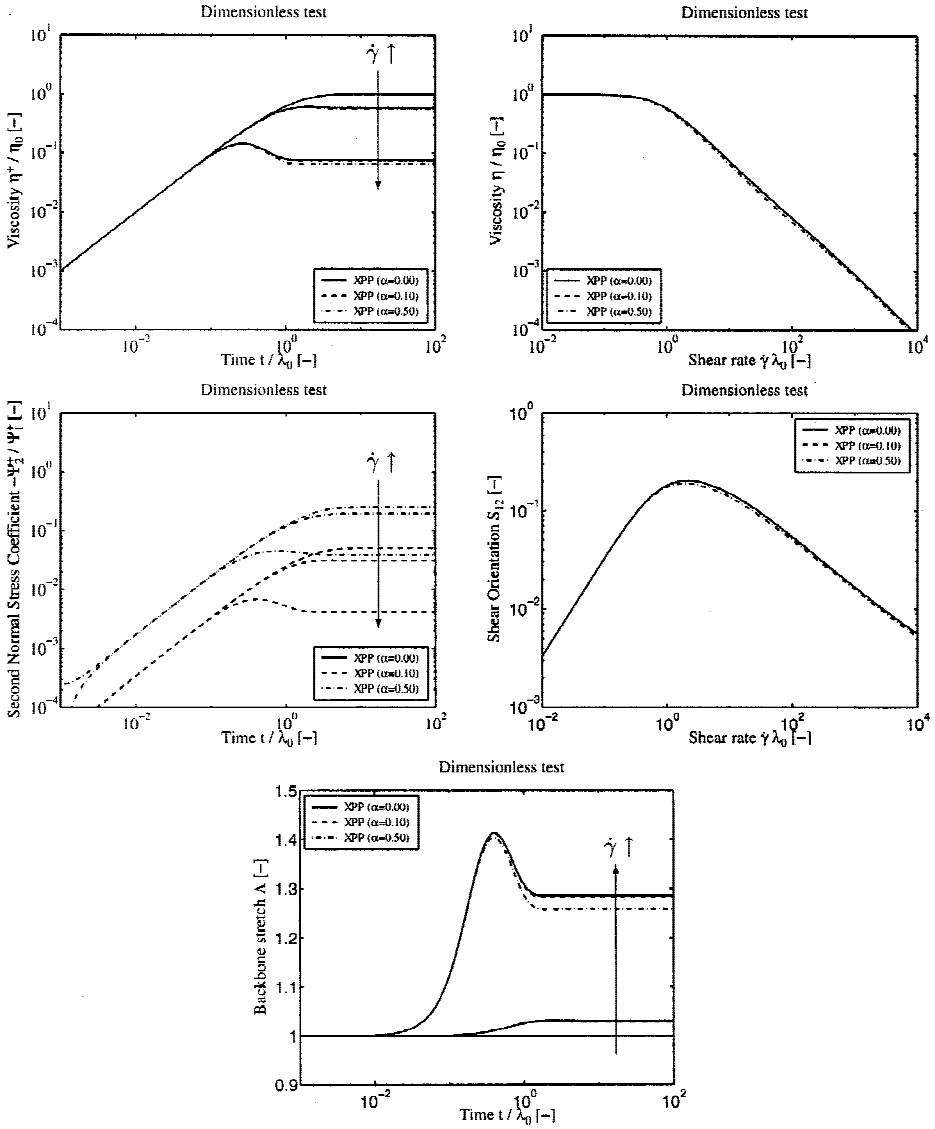

FIG. 3. Dimensionless features in simple shear flow for the XPP model: transient viscosity (*left top*), steady state viscosity (*right top*), transient second over first normal stress coefficient ratio $-\Psi_2/\Psi_1$ (*left middle*), steady state shear orientation component S_{12} (*right middle*) and transient backbone stretch Λ (*bottom*). Parameters: $q = 5$; $\lambda_{0s} = (150/912)\lambda_{0b}$; $\alpha = 0{,}0.1{,}0.5$. Transient: $\gamma = 10^{-5}$, 1, 10.

We would like to point out, that the transient and steady state uniaxial and equibiaxial viscosities show similar behavior as the first planar viscosity. As in simple shear the influence of parameter α is rather small. More figures may be found in EPAPS Document No. E-JORHD2-45-013104.

IV. PERFORMANCE OF THE MULTIMODAL POM–POM MODEL

For three different materials, the performance of the *extended Pom–Pom* model in multimode form is investigated and compared with experimental data. Here, the full

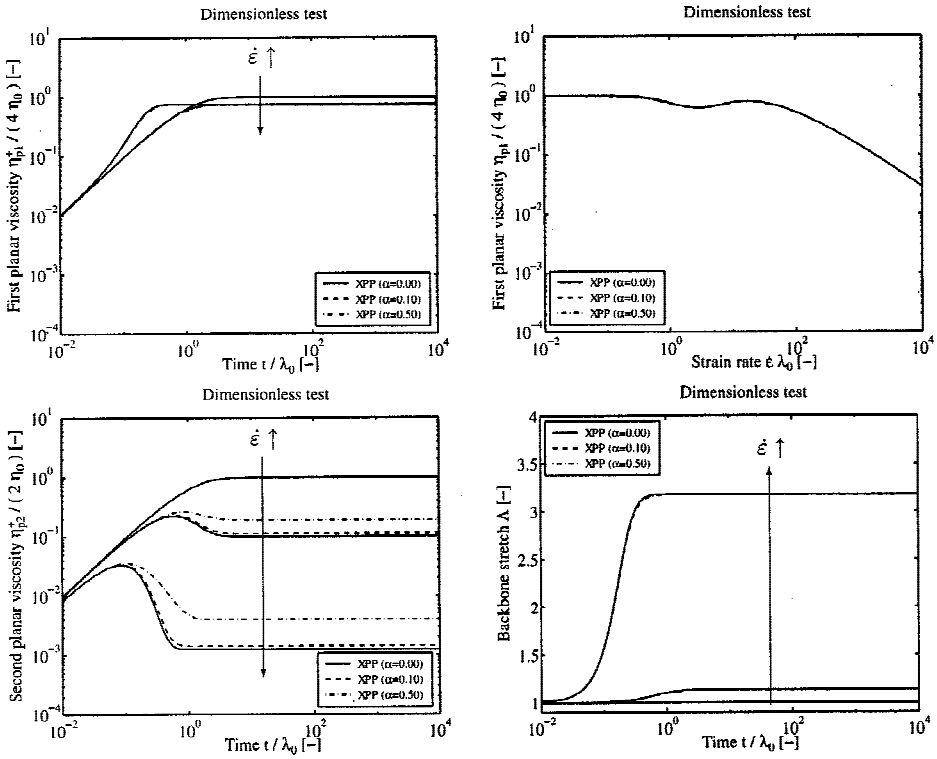

FIG. 4. Dimensionless features in planar elongational flow for the XPP model: transient (*left top*) and steady state (*right top*) first planar viscosity η_{p1}, transient second planar viscosity η_{p2} (*left bottom*), and transient backbone stretch Λ (*right bottom*). Parameters: $q = 5$; $\lambda_{0s} = (150/912)\lambda_{0b}$; $\alpha = 0$, 0.1, 0.5. Transient: $\varepsilon = 10^{-5}$, 1, 10.

results will be shown for only one material to emphasize our point. For the other two materials, the main results are summarized and the interested reader is referred to EPAPS Document No. E-JORHD2-45-013104 for further information.

For all materials, the linear parameters, i.e., backbone relaxation time λ_{0b} and modulus G_0, are determined from dynamic measurements. The data for BASF Lupolen 1810H (681 133 256, stabilized with S4918) LDPE melt will be shown in an extensive comparison. This LDPE melt has been characterized by Hachmann (1996) and Kraft (1996). As a second LDPE melt, the IUPAC A melt was investigated, which has been well characterized by Meissner (1972, 1975) and Münstedt and Laun (1979). Finally, the Statoil 870H (85579, stabilized with S5011) HDPE melt has been investigated, also characterized by Hachmann (1996) and Kraft (1996). This last material is chosen to see how the *Pom–Pom* model, developed for long-chain branched materials, performs for a material with a different molecular structure.

Fitting of the nonlinear parameters is done manually. Some physical guidelines are taken into account for that. For a branched molecule, going from the free ends inwards, an increasing number of arms is attached to every backbone of the representative pom–pom. The relaxation time of a backbone segment is determined by the distance to the nearest free end that is able to release it from its tube constraint by retraction. Towards the middle of a complex molecule, the relaxation time is exponentially increasing. So, the parameter q_i, denoting the number of arms for every backbone segment, and the orien-

TABLE III. XPP parameters for fitting of the Lupolen 1810H melt. $T_r = 150\,°\text{C}$, $\nu_i = 2/q_i$. Activation energy: $E_0 = 58.6\,\text{kJ/mol}$.

	Maxwell parameters		XPP model		
i	$G_{0,i}$ (Pa)	$\lambda_{0b,i}$ (s)	q_i	ratio: $\lambda_{0b,i}/\lambda_{0s,i}$	α_i
1	2.1662×10^{4}	1.0000×10^{-1}	1	3.5	0.350
2	9.9545×10^{3}	6.3096×10^{-1}	2	3.0	0.300
3	3.7775×10^{3}	3.9811×10^{0}	3	2.8	0.250
4	9.6955×10^{2}	2.5119×10^{1}	7	2.8	0.200
5	1.1834×10^{2}	1.5849×10^{2}	8	1.5	0.100
6	4.1614×10^{0}	1.0000×10^{3}	37	1.5	0.005

tation relaxation time $\lambda_{0b,i}$ are increasing towards the center of the molecule. The stretch relaxation time $\lambda_{0s,i}$ is physically constrained to lie in the interval $\lambda_{0b,i-1} < \lambda_{0s,i} \leqslant \lambda_{0b,i}$ [Inkson *et al.* (1999)].

A. BASF Lupolen 1810H LDPE melt

This LDPE melt has been characterized in elongation by Hachmann (1996). All elongational components have been measured: first and second planar, uniaxial and equibiaxial elongational viscosities. Kraft (1996) characterized the material in shear, both shear viscosity and first normal stress coefficient, and also measured a reversed flow. All measurements, shear and elongation, were carried out at a temperature of $T = 150\,°\text{C}$. The linear parameters λ_{0b} and G_0 have been calculated from a continuous relaxation spectrum determined by Hachmann (1996). With the given activation energy E_0, the temperature dependence can be calculated using the following equation [Ferry (1980)]:

$$\ln\left[\frac{\eta_0(T)}{\eta_0(T_r)}\right] = \ln\left(\frac{a_T}{b_T}\right) = \frac{E_0}{R}\left(\frac{1}{T} - \frac{1}{T_r}\right). \tag{32}$$

Here, R is the gas constant, T_r is the reference temperature, and T is the temperature where to shift to, both in kelvin. The nonlinear parameters q and λ_{0s} *are fitted on the uniaxial elongational data only*. Since the parameter α has almost no influence on uniaxial viscosity, shear viscosity and shear first normal stress coefficient, it can solely be used to fit the second normal stress coefficient (if available) or, like with this material, to the second planar viscosity data. We expect anisotropy to decrease from the free ends inwards. As can be seen in Table III, which gives the linear and nonlinear parameters, our expectations are in agreement with the fit. If there is no second normal stress difference or second planar viscosity data available, as a guideline, anisotropy parameter α could be chosen as $0.1/q$, since more arms (parameter q) are attached to the branch points while going towards the center of the molecule and thus diminishing α.

The uniaxial data and fits are plotted in Fig. 5. The model does an excellent job in modeling the experimental data. The final points of the transient experimental data are taken as the steady state data points, and shown in the inset. As most probably the true steady state values have not been reached yet, these are quasisteady state data points.

Figure 6 shows the predictions for the transient and quasisteady state first and second planar viscosity. Again, a good agreement between experiments and calculations is obtained for the first planar viscosity.

For the second planar viscosity, quantitative agreement is poorer, although qualitatively a good trend is seen (thinning instead of thickening behavior). The numerical

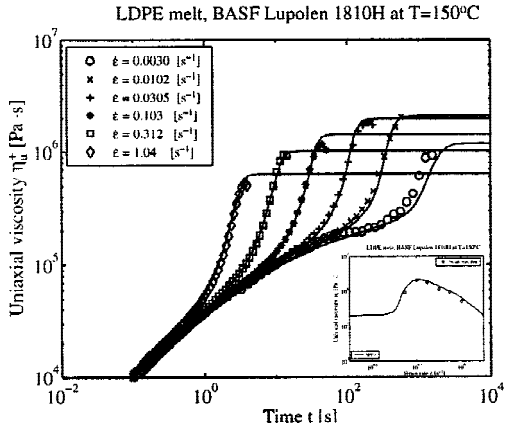

FIG. 5. Transient and quasisteady state (*inset*) uniaxial elongational viscosity η_u of the XPP model for Lupolen 1810H melt at $T = 150\,°\text{C}$. $\nu_i = 2/q_i$, $\varepsilon = 0.0030,\ 0.0102,\ 0.0305,\ 0.103,\ 0.312,\ 1.04\ \text{s}^{-1}$.

results underpredict the experimental data. There are three possible reasons for this. First, it is rather difficult to obtain accurate experimental results. Second, better numerical results might be obtained by starting off with more modes. And third, a change in the orientation evolution equation might improve predictions, too. The last two remarks are supported by the unphysically ''bumpy'' behavior of the steady state values.

The transient and quasisteady state equibiaxial experimental data and the calculated results are depicted in Fig. 7. Again, the experimental data is predicted rather well. However, a small delay in time for the upswing can be noticed. A remarkable feature is that the model first predicts a drop under the zero shear rate viscosity line, followed by elongational thickening. This can also be seen in the experimental data.

Figure 8 shows the experimental and model results of the shear viscosity and first normal stress coefficient. It is obvious that the model is giving an excellent prediction for the shear viscosity. For the first normal stress coefficient, the model is predicting the experimental data good. Notice, that the overshoot is not so pronounced as for the ex-

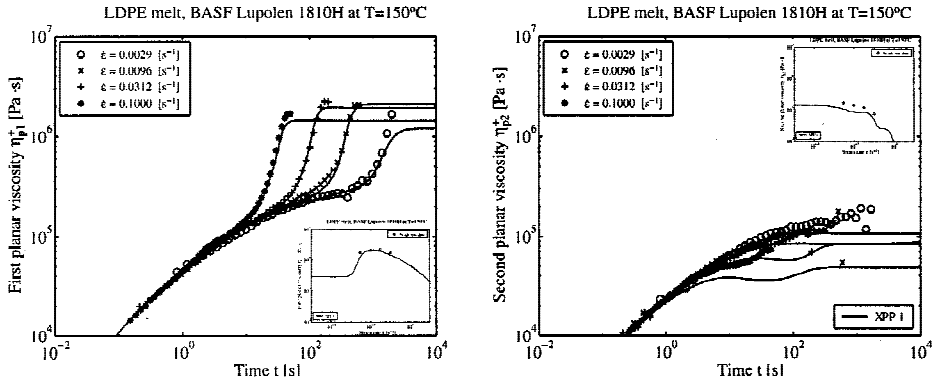

FIG. 6. Transient and quasisteady state (*inset*) first planar elongational viscosity η_{p1} (*left*) and second planar elongational viscosity η_{p2} (*right*) of the XPP model for Lupolen 1810H melt at $T = 150\,°\text{C}$. $\nu_i = 2/q_i$, $\varepsilon = 0.0029,\ 0.0096,\ 0.0312,\ 0.1000\,\text{s}^{-1}$.

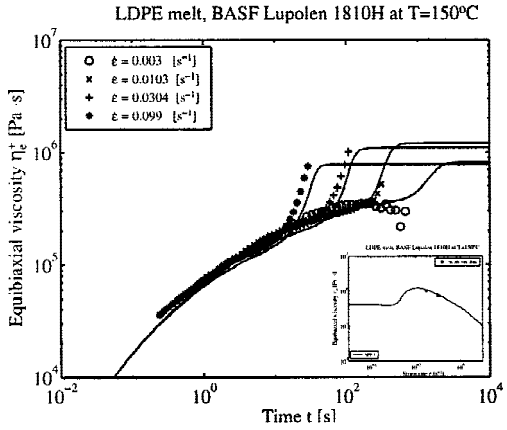

FIG. 7. Transient and quasisteady state (*inset*) equibiaxial elongational viscosity η_e of the XPP model for Lupolen 1810H melt at $T = 150\,°\text{C}$. $\nu_i = 2/q_i$. $\varepsilon = 0.003,\ 0.0103,\ 0.0304,\ 0.099\ \text{s}^{-1}$.

perimental data. If the transient plots are carefully examined, the different modes can be noted. This is caused by the relaxation times being just a little too far apart.

Figure 9 shows the experimental results for a reversed shear flow and the model predictions. In this reversed flow, a strain rate of $\gamma = 1\ \text{s}^{-1}$ is applied in one direction. After a certain amount of time t^* the strain rate is reversed and applied in opposite direction. For details on the reversed flow, see Kraft (1996). The orientation angle plotted in the third picture of the figures, is defined as

$$\chi = \frac{1}{2}\arctan\left(\frac{2\tau_{12}}{N_1}\right). \tag{33}$$

All features seen in the experiments are predicted. For the shear stress, in case of short reverse time or preshearing, the values change sign and go through a minimum before reaching the steady state value. For higher reverse times or preshearing, the curves change sign and then directly reach the steady state value, without going through a

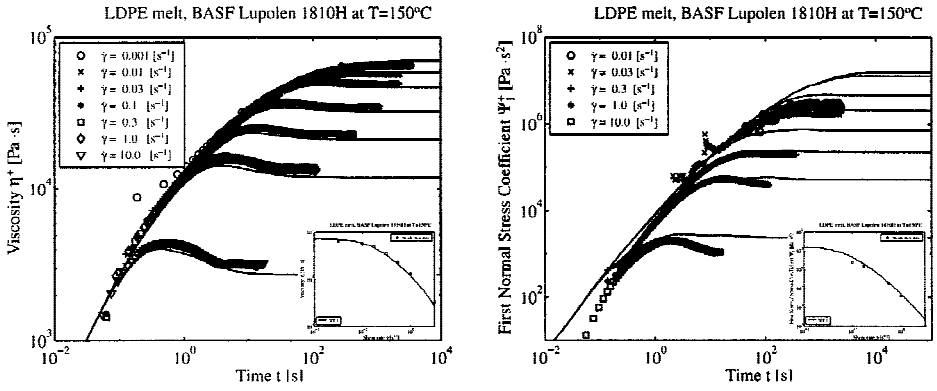

FIG. 8. Transient and steady state (*inset*) shear viscosity η (*left*) and first normal stress coefficient Ψ_1 (*right*) of the XPP model for Lupolen 1810H melt at $T = 150\,°\text{C}$. $\nu_i = 2/q_i$. $\gamma = 0.001,\ 0.01,\ 0.03,\ 0.1,\ 0.3,\ 1,\ 10\ \text{s}^{-1}$.

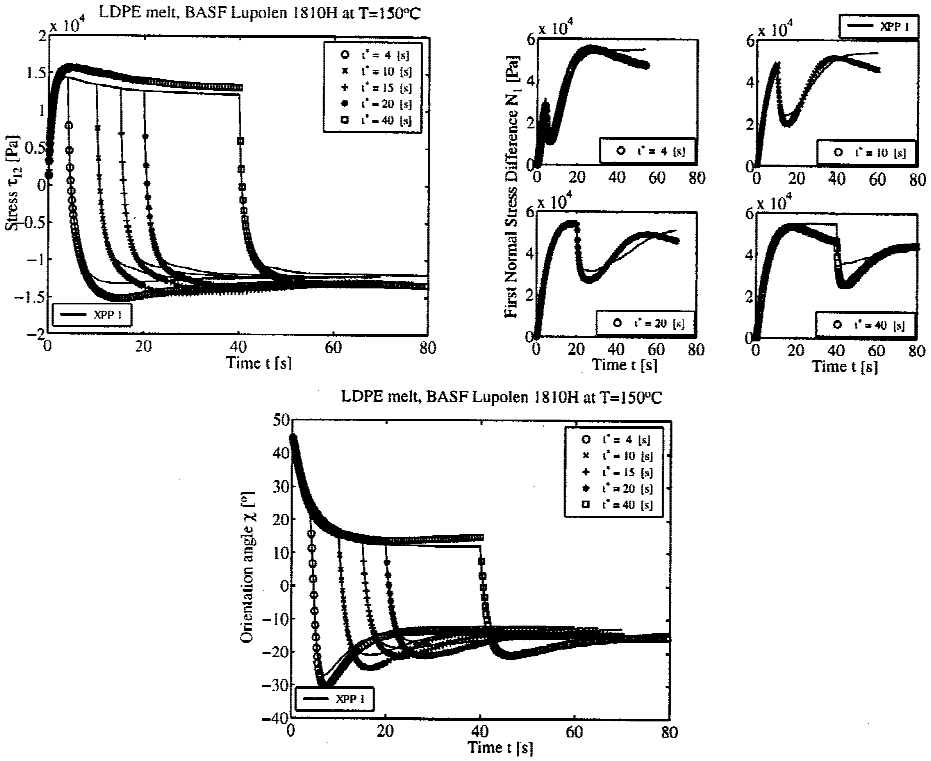

FIG. 9. Reversed flow of the XPP model for Lupolen 1810H melt at $T = 150\,^{\circ}\mathrm{C}$ and $\gamma = 1\ \mathrm{s}^{-1}$. Shear stress τ_{12} (*left,top*), first normal stress difference N_1 (*right,top*) and orientation angle χ (*bottom*) for different initial strains $\gamma - \gamma t^*$. $t^* = 4,\ 10,\ 15,\ 20,\ 40\ \mathrm{s}^{-1}$.

minimum first. In case of the first normal stress difference, the curves go through a minimum after preshearing and then, as should be, return to the original curve seen if no preshearing has occurred. For the predictions, the different modes can be seen as small wiggles just after reversing the flow. We speculate that this might be improved by increasing the amount of modes or a change in the orientation evolution equation. The orientation angle changes sign, just like the shear stress. However, these curves always show a minimum.

In general, a good quantitative agreement is obtained in this reversed flow, and only the first normal stress difference shows some deviations. Notice however, that in this case the plots are on a linear scale, while all other plots are on a logarithmic scale.

It should be pointed out again, that all parameters where fitted onto the uniaxial data only, while only six modes where used. The linear parameters determine the basics of all curves and therefore should be chosen carefully.

For a second LDPE material, the well characterized IUPAC A LDPE melt [uniaxial data from Münstedt and Laun (1979) and shear data from Meissner (1975)], the same fitting procedure is applied (see EPAPS Document No. E-JORHD2-45-013104). The uniaxial experimental data is predicted excellent, while good to excellent results are obtained in shear.

As a last remark, it should be noted that the nonlinear parameters have a larger influence on elongation than on shear. Therefore, by fitting the other way around, i.e., first on the shear data, it is not obvious, that good fits will be obtained in elongation.

TABLE IV. XPP parameters for fitting of the Statoil 870H HDPE melt. $T_r = 170\,°\text{C}$. $\nu_i = 2/q_i$. Activation energy: $E_0 = 27.0$ kJ/mol.

	Maxwell parameters		XPP model		
i	$G_{0,i}$ (Pa)	$\lambda_{0b,i}$ (s)	q_i	ratio: $\lambda_{0b,i}/\lambda_{0s,i}$	α_i
1	1.5350×10^{5}	1.0000×10^{-2}	1	6.0	0.50
2	3.1870×10^{4}	1.0000×10^{-1}	1	5.0	0.50
3	7.8180×10^{3}	1.0000×10^{0}	1	4.0	0.50
4	1.4130×10^{3}	1.0000×10^{1}	2	3.0	0.40
5	1.9680×10^{2}	1.0000×10^{2}	4	2.0	0.30
6	2.0650×10^{1}	1.0000×10^{3}	7	2.0	0.13
7	9.3000×10^{0}	5.0000×10^{3}	5	2.5	0.25

B. Statoil 870H HDPE melt

Hachmann (1996) has measured the elongational viscosities for this HDPE melt. The experiments were carried out at a temperature of $T = 150\,°\text{C}$. In shear, the material is characterized by Kraft (1996) at a temperature of $T = 170\,°\text{C}$. The discrete spectrum of seven relaxation times and moduli is given by Wagner *et al.* (1998) at $T = 170\,°\text{C}$. The nonlinear parameters q and ratio $\lambda_{0b}/\lambda_{0s}$ are manually fitted on the uniaxial elongational data only. The nonlinear parameter α is again fitted on the second planar viscosity data. The linear and nonlinear parameters for this material at a temperature of $T = 170\,°\text{C}$ are given in Table IV. The shift in temperature can be determined using Eq. (32) and the activation energy given in Table IV.

To our surprise even for a HDPE melt the model gives a satisfactory agreement with the uniaxial experimental data, as can be seen in Fig. 10. The model shows an upswing which is a bit sooner in time than the experimental data. This might indicate that a change in the stretch evolution equation is necessary for linear polymers. Notice that the highest q for this HDPE material ($q = 7$) is significantly lower than for the LDPE melt ($q = 37$). Theoretically, for an HDPE melt $q = 1$ is expected for all modes. However, this does not give sufficient elongational thickening behavior. The physical interpretation of q, the amount of arms attached to the backbone, is therefore only partly followed. Maybe a

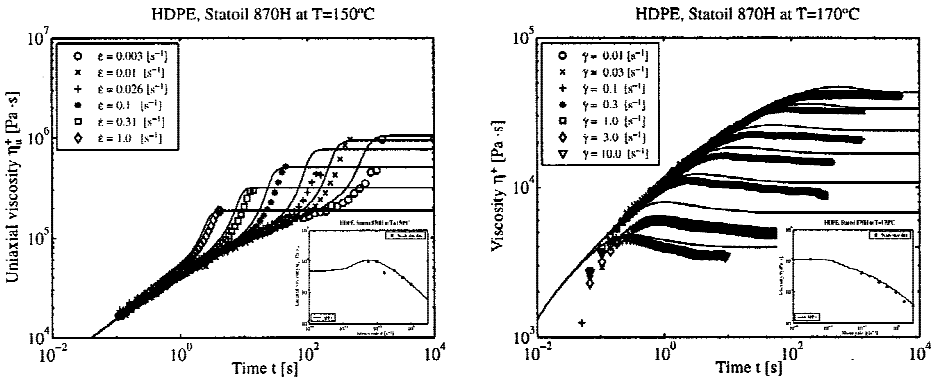

FIG. 10. Transient (*left*) and quasisteady state (*inset*) uniaxial elongational viscosity η_u at $T = 150\,°\text{C}$, and transient (*right*) and steady state (*inset*) shear viscosity η_s at $T = 170\,°\text{C}$ of the XPP model for Statoil 870H HDPE melt. $\nu_i = 2/q_i$. $\varepsilon = 0.003$, 0.010, 0.026, 0.10, 0.31, $1.0\ \text{s}^{-1}$. $\gamma = 0.01$, 0.03, 0.1, 0.3, 1.0, 3.0, $10.0\ \text{s}^{-1}$.

more physical picture can be sketched for parameter ν. It could be regarded as the amount of influence that the polymer material after the branchpoint, i.e., the ''arms,'' has on the contribution to the stretch of the considered backbone tube between two branchpoints. A long linear polymer chains could be entangled in the surrounding polymer chains, such that it is equally contributing to the stretch as seven branched short polymer chain arms.

For the first planar elongational viscosity good agreement is obtained. For the second planar elongational viscosity data the model underpredicts the data, just as for the Lupolen LDPE melt. However, qualitative agreement, i.e., elongational thinning, is accounted for. The different modes can be seen for the steady state solution, which indicates that not enough modes are used. Improvement might also be obtained by a change in the orientation evolution equation. Good agreement is observed between the experimental and calculated data for the equibiaxial elongational viscosity.

This HPDE melt is very elastic and it is difficult to capture the zero-shear viscosity with start-up shear experiments. Therefore it is determined by creep experiments [Kraft (1996)]. This also means that it is difficult to identify a satisfying relaxation spectrum. The shear viscosity response is shown in Fig. 10. Although steady state predictions are reasonable, transient predictions are a bit off; the experimental overshoot is overpredicted. The model also overpredicts the end steady state values a bit. For the first normal stress coefficient in shear, the model predicts the right shape, but is mostly overpredicting transient start-up experimental data. For only fitting on the uniaxial data, the predictions in shear are still good. The interested reader can find more graphical support for this subsection in EPAPS Document No. E-JORHD2-45-013104.

In general, it can be stated that the *Pom–Pom* model, although developed for branched molecules, is quite capable of predicting the experimental data of the linear HDPE melt over the full range of different experiments. In elongation the prediction is good, while for shear the model somewhat overpredicts the experimental data. It is mentioned again that the zero-shear viscosity and the linear spectrum for this material are difficult to identify, as it is a highly elastic material. Besides, all parameters where fitted manually where better results may be obtained by an automatic generation of the parameters. Another improvement may be reached by a slight adjustment of the evolution of stretch or orientation equation, in such a way, that it is more in agreement with the molecular topology of an HDPE melt.

V. CONCLUSIONS

The *extended Pom–Pom* model discussed here can quantitatively describe the behavior in simple flows for two different commercial LDPE melts. All flow components can be predicted satisfactorily by manually fitting the nonlinear parameters *on the uniaxial experimental data only*. Improvements have been made compared with previous versions of the *Pom–Pom* model. By eliminating the finite extensibility condition from the original equations, the model predictions are now smooth and more realistic. Moreover, a second normal stress difference is introduced, which was not present in the differential form of McLeish and Larson (1998).

The XPP model shows a too pronounced thinning for the second planar viscosity. We speculate, that this might be improved by a change in the orientation evolution equation.

For a third material, a HDPE melt, the model predicts the experimental data in a satisfactory way. The elongational experimental data, which is used to fit the nonlinear parameters, is described well. For shear the experimental data is slightly overpredicted. However, it should be pointed out, that the model was mainly developed for polymers with long-chain branches, such as LDPE melts. As HDPE has a different molecular

structure, better results may be obtained by adjusting the stretch and orientation equations in such a way that they closer match the molecular topology of HDPE melts. However, it is still quite satisfying to notice, that even for an HDPE melt, the model is doing a good job.

An important aspect for a good description of the experimental data is the linear discrete relaxation spectrum. This spectrum defines how well the linear viscoelastic curve is followed. A good basis for nonlinear rheology of commercial polymer melts is the right choice of the discrete linear relaxation spectrum.

Improvements of the fits shown here can be obtained by determining the parameters with a more advanced fit procedure. All nonlinear parameters were determined manually by following some basic ground rules as given by McLeish and Larson (1998), Inkson *et al.* (1999). Only the uniaxial and second planar experimental data was used for fitting. Although it is satisfying that the other data is predicted so well (regarding that it was not used for fitting), better predictions may be expected, if all data is taken in consideration using an automated identification procedure.

In general, it can be noted, that a good basic ground is laid for calculating commercial polymer melts with the multimode differential constitutive *Pom–Pom* model, but there is still room for improvement.

ACKNOWLEDGMENTS

Financial support from the Commission of the European Union through the BRITE-EuRAM III project ART (BE96-3490) is gratefully acknowledged. Also, the authors would like to thank the reviewers for their constructive comments.

APPENDIX A: REWRITE PROCEDURE FOR THE ORIENTATION EQUATION

As a starting point, the equation for the auxiliary tensor A is taken

$$\overset{\nabla}{A}+\frac{1}{\lambda_{0b}}\left(A-\frac{1}{3}I\right)=0\Leftrightarrow\dot{A}=L\cdot A+A\cdot L^{T}-\frac{1}{\lambda_{0b}}\left(A-\frac{1}{3}I\right). \tag{A1}$$

To get to the backbone orientation tensor S, the auxiliary tensor A is divided by its trace

$$S=\frac{A}{I_A}\Leftrightarrow A=I_A S. \tag{A2}$$

Now, the time derivative of Eq. (A2) is taken

$$\dot{A}=\dot{I}_A S+I_A\dot{S}. \tag{A3}$$

As $\dot{I}_A=I_{\dot{A}}$ holds, for the time derivative of the trace of auxiliary tensor A, the trace of equation (A1) is taken

$$I_{\dot{A}}=2(D:A)-\frac{1}{\lambda_{0b}}(I_A-1). \tag{A4}$$

If the Eqs. (A2), (A3), and (A4) are substituted into Eq. (A1), the following relation occurs:

$$I_{\dot{A}}S+I_A\dot{S}=L\cdot A+A\cdot L^{T}-\frac{1}{\lambda_{0b}}\left(A-\frac{1}{3}I\right), \tag{A5}$$

which can also be written as

$$2(D{:}I_AS)S-\frac{1}{\lambda_{0b}}(I_AS-S)+I_AS = I_AL\cdot S+I_AS\cdot L^T-\frac{1}{\lambda_{0b}}\left(I_AS-\frac{1}{3}I\right). \tag{A6}$$

By dividing this last equation with the trace of the auxiliary tensor A, it reduces to

$$\overset{\nabla}{S}+2(D{:}S)S+\frac{1}{\lambda_{0b}I_A}\left(S-\frac{1}{3}I\right) = 0. \tag{A7}$$

APPENDIX B: ENHANCED POM–POM MODELS ACCORDING TO ÖTTINGER (2000)

The Green–Kubo type expression for the orientation equation as proposed by Öttinger reads

$$\overset{\nabla}{A}+\frac{1}{\lambda_b}I_A\left[(3S+\alpha_1I+\alpha_2S^{-1})\cdot\left(S-\frac{1}{3}I\right)+(\alpha_3I+\alpha_4S)\mathrm{tr}\left(I-\frac{1}{3}S^{-1}\right)\right] = 0, \quad S = \frac{A}{I_A}, \tag{B1}$$

where α_1, α_2, $\alpha_3 \geqslant 0$ and α_4 is arbitrary. Öttinger suggested that, for numerical purposes, it may be convenient to suppress all occurrences of S^{-1} by choosing $\alpha_2 = \alpha_3 = \alpha_4 = 0$. Equation (B1) then reduces to

$$\overset{\nabla}{A}+\frac{1}{\lambda_b}I_A\left[3S\cdot S+(\alpha_1-1)S-\frac{1}{3}\alpha_1I\right] = 0, \quad S = \frac{A}{I_A}. \tag{B2}$$

Although he did not mention this, in this case, to correctly describe linear viscoelasticity, the relaxation time for the backbone tube orientation must be chosen as $\lambda_b = \lambda_{0b}(1+\alpha_1)$, where λ_{0b} is obtained from dynamic measurements. The attention is drawn to the fact that for zero α_1, still a second normal stress difference Ψ_2 is present. By increasing α_1, Ψ_2 is decreased, which is opposite to the XPP model.

The set of Eqs. (3), (4), and (B2) can also be written as a single equation

$$\overset{\nabla}{\tau}+\lambda_1(\tau)^{-1}\tau = 2G_0D, \tag{B3}$$

with

$$\lambda_1(\tau)^{-1} = \frac{1}{\lambda_b}\left\{\frac{1}{G_0\Lambda^2}\tau+f_1(\tau)^{-1}I+G_0\left[f_1(\tau)^{-1}-\frac{1+\alpha_1\Lambda^4}{\Lambda^2}\right]\tau^{-1}\right\}, \tag{B4}$$

$$\frac{1}{\lambda_b}f_1(\tau)^{-1} = \frac{2}{\lambda_s}\left(1-\frac{1}{\Lambda}\right)+\frac{1}{\lambda_b}\left(\frac{1}{\Lambda^4}+\alpha_1-\frac{I_{\tau\cdot\tau}}{3G_0^2\Lambda^4}\right), \tag{B5}$$

and

$$\Lambda = \sqrt{1+\frac{I_\tau}{3G_0}}, \quad \lambda_s = \lambda_{0s}e^{-\nu(\Lambda-1)}, \quad \nu = \frac{2}{q}. \tag{B6}$$

Again, the different parts for stretch and orientation can be detected. The extra stress Eq. (B3) is referred to as the *single-equation improved Pom–Pom* (SIPP) model.

The combined set of the orientation Eq. (B2), the stretch Eq. (3) and the extra stress Eq. (4) is referred to as the *double-equation improved Pom–Pom* (DIPP) model. The addition *improved* is used to point out that local branch-point displacement is incorpo-

TABLE V. DIPP equation set.

DIPP model
Viscoelastic stress $\tau = G_0(3\Lambda^2 S - I).$
Evolution of orientation $\overset{\nabla}{A} + \frac{1}{\lambda_b} I_A \left[3S\cdot S + (\alpha_1 - 1)S - \frac{1}{3}\alpha_1 I \right] = 0, \quad S = \frac{A}{I_A}, \quad \lambda_b = \lambda_{0b}(1+\alpha_1).$
Evolution of the backbone stretch $\dot{\Lambda} = \Lambda[D:S] - \frac{1}{\lambda_s}(\Lambda - 1), \quad \lambda_s = \lambda_{0s} e^{-\nu(\Lambda-1)}, \quad \nu = \frac{2}{q}.$

rated in the model [Blackwell *et al.* (2000)]. The finite extensibility condition ($\Lambda \leqslant q$) has been taken out for reasons mentioned earlier. For the DIPP model, it is pointed out, that within a coupled Finite Element method, extra boundary conditions are needed for Λ and S. For convenience, an overview is given of the equations for the two models in Tables V and VI.

It should be mentioned that these two models show numerical problems (they are suspected to have a bifurcation), and for the rest they give similar results as the XPP model.

TABLE VI. SIPP equation set.

Single-equation improved *Pom-Pom* (SIPP) model
Viscoelastic stress $\overset{\nabla}{\tau} + \lambda_1(\tau)^{-1}\tau = 2G_0 D.$
Relaxation time tensor $\lambda_1(\tau)^{-1} = \frac{1}{\lambda_b}\left\{ \frac{1}{G_0\Lambda^2}\tau + f_1(\tau)^{-1} I + G_0 \left[f_1(\tau)^{-1} - \frac{1+\alpha_1\Lambda^4}{\Lambda^2} \right] \tau^{-1} \right\},$ $\lambda_b = \lambda_{0b}(1+\alpha_1).$
Extra function $\frac{1}{\lambda_b} f_1(\tau)^{-1} = \frac{2}{\lambda_s}\left(1 - \frac{1}{\Lambda}\right) + \frac{1}{\lambda_b}\left(\frac{1}{\Lambda^4} + \alpha_1 - \frac{I_{\tau\tau}}{3G_0^2\Lambda^4}\right).$
Backbone stretch and stretch relaxation time $\Lambda = \sqrt{1 + \frac{I_\tau}{3G_0}}, \quad \lambda_s = \lambda_{0s} e^{-\nu(\Lambda-1)}, \quad \nu = \frac{2}{q}.$

References

Bishko, G. B., O. G. Harlen, T. C. B. McLeish, and T. M. Nicholson, ''Numerical simulation of the transient flow of branched polymer melts through a planar contraction using the 'pom-pom' model,'' J. Non-Newtonian Fluid Mech. **82**, 255–273 (1999).

Blackwell, R. J., T. C. B. McLeish, and O. G. Harlen, ''Molecular drag-strain coupling in branched polymer melts,'' J. Rheol. **44**, 121–136 (2000).

Debbaut, B. and J. Dooley, ''Secondary motions in straight and tapered channels: Experiments and three-dimensional finite element simulation with a multimode differential viscoelastic model,'' J. Rheol. **43**, 1525–1545 (1999).

Doufas, A. K., I. S. Dairanieh, and A. J. McHugh, ''A continuum model for flow-induced crystallization of polymer melts,'' J. Rheol. **43**, 85–109 (1999).

Ferry, J. D., *Viscoelastic Properties of Polymers*, 3rd ed. (Wiley, New York, 1980).

Hachmann, P., ''Multiaxiale Dehnung von Polymerschmelzen,'' Ph.D. thesis, Dissertation ETH Zürich Nr. 11890, 1996.

Inkson, N. J., T. C. B. McLeish, O. G. Harlen, and D. J. Groves, ''Predicting low density polyethylene rheology in flows and shear with Pom-Pom constitutive equation,'' J. Rheol. **43**, 873–896.

Jerschow, P. and H. Janeschitz-Kriegl, ''On the development of oblong particles as precursors for polymer crystallization from shear flow: Origin of the so-called fine grained layers,'' Rheol. Acta **35**, 127–133 (1996).

Kalogrianitis, S. G. and J. W. van Egmond, ''Full tensor optical rheometry of polymer fluids,'' J. Rheol. **41**, 343–364 (1997).

Kraft, M., ''Untersuchungen zur scherinduzierten rheologischen Anisotropie von verschiedenen Polyethylen-Schmelzen,'' Ph.D. thesis, Dissertation ETH Zürich Nr. 11417, 1996.

Larson, R. G., ''Review: Instabilities in viscoelastic flows,'' Rheol. Acta **31**, 213–263 (1992).

McLeish, T. C. B. and R. G. Larson, ''Molecular constitutive equations for a class of branched polymers: The pom-pom polymer,'' J. Rheol. **42**, 81–110 (1998).

Meissner, J., ''Modifications of the Weissenberg rheogoniometer for measurement of transient rheological properties of molten polyethylene under shear. Comparison with tensile data,'' J. Appl. Polym. Sci. **16**, 2877–2899 (1972).

Meissner, J., ''Basic parameters, melt rheology, processing and end use properties of three similar low density polyethylene samples,'' Pure Appl. Chem. **42**, 553–612 (1975).

Münstedt, H. and H. M. Laun, ''Elongational behaviour of a low density polyethylene melt II,'' Rheol. Acta **18**, 492–504 (1979).

Öttinger, H. C., ''Capitalizing on nonequilibrium thermodynamics: branched polymers,'' in Proceedings of the XIIIth International Congress on Rheology, Cambridge, UK, August 2000.

Peters, G. W. M. and F. P. T. Baaijens, ''Modelling of non-isothermal viscoelastic flows,'' J. Non-Newtonian Fluid Mech. **68**, 205–224 (1997).

Rubio, P. and M. H. Wagner, ''Letter to the Editor: A note added to 'Molecular constitutive equations for a class of branched polymers: The pom-pom polymer,' '' [J. Rheol. **42**, 81 (1998)], J. Rheol. **43**, 1709–1710 (1999).

See EPAPS Document No. E-JORHD2-45-013104 for sixteen figures of the XPP model. This document may be retrieved via the EPAPS homepage (http://www.aip.org/pubservs/epaps.html) or from ftp.aip.org in the directory/epaps/. See the EPAPS homepage for more information.

Wagner, M. H., H. Bastian, P. Ehrecke, M. Kraft, P. Hachmann, and J. Meissner, ''Nonlinear viscoelastic characterization of a linear polyethylene (HPDE) melt in rotational and irrotational flows,'' J. Non-Newtonian Fluid Mech. **79**, 283–296 (1998).